arXiv:cond-mat/0208316v1 [cond-mat.mtrl-sci] 15 Aug 2002

First Principles Studies of $KNbO_3$, $KTaO_3$ and $LiTaO_3$ Solid Solutions

Serguei Prosandeev, Eric Cockayne and Benjamin Burton

Ceramics Division, Materials Science and Engineering Laboratory, National Institute of Standards and Technology, Gaithersburg, MD 20899-8520

Abstract.

$KTaO_3$-based solid solutions exhibit a variety of interesting physical phenomena. To better understand these phenomena, we performed first-principles calculations on $[K_{1-x},Li_x]TaO_3$ (KLT) and $K[Ta_{1-x},Nb_x]O_3$ (KTN) supercells. Our results show Li displacements and potential barrier heights in KLT that are in excellent agreement with values obtained from experimental fits. Dramatic changes in B-site dynamical charges occur in KTN in response to changes in near neighbor (nn) coordination. These effects can be explained by heterogeneity in the local electronic dielectric permittivity.

INTRODUCTION

$KTaO_3$ (KT) is one of the rare perovskite-type materials that remains cubic down to zero Kelvin. It is also interesting because it is a quantum paraelectric and, therefore, its ferroelectric phase transition at low temperatures is suppressed by zero-point quantum vibrations. $KNbO_3$ (KN) is ferroelectric even at room temperature and exhibits a series of ferroelectric phase transitions with decreasing temperature. A variety of interesting phenomena occur when KT or/and KN form solid solutions via isovalent substitution of A or B cations; $[K_{1-x},Li_x]TaO_3$ (KLT) and $K[Ta_{1-x},Nb_x]O_3$ (KTN) are solid solutions which exhibit both order-disorder and soft-mode characteristics. In this work, we use first-principles supercell calculations to investigate lattice dynamics, ground-state structures, and dynamical effective charges in KLT and KTN.

Recent developments in quantum theory of polarization (see the review in [1]) allow one to make first-principle (FP) computations of polarization and its derivative, dynamical charge. Such computations show that dynamical charges are anomalously large in ferroelectric perovskite-type crystals (see e.g. Ref. [2]), and this has a significant effect on the soft-mode behaviors of these materials. Variations of dynamical charges as functions of local chemical coordination, as occurs in solid solutions, have not been extensively studied. We present systematic results on

the dynamical charges as functions of chemical configurations in KTN. The same tendencies were found for PMN supercells.

METHODS

We use the Vienna *ab initio* simulation package (VASP) [3,4], which treats electronic structure within the framework of density function theory. Detailed computations were performed for 40 ion supercells and a limited number of computations were done for an 80 ion supercell. The basis vectors were [002], [020] and [200] for the 40 atom cell (KLT40), and [220], [022] and [202] for the 80 atom cell. The k-vector mesh was constructed from 4x4x4 Monkhorst-Pack grid. Verification of this computational scheme was performed for pure $KTaO_3$; the self-consistent lattice constant $a = 3.96$ Å agrees with previous LDA and GGA computations [5]. The calculated lattice constant is smaller than the experimental value $a = 3.983$ Å [6].

VASP computes interatomic forces and total energies for crystals, and allows global relaxation as well as constrained relaxation of chosen internal coordinates and/or lattice parameters. We used frozen-phonon methods to obtain force constants for computing lattice dynamics. To compute dynamical charges, we used Berry phase analyses as implemented in the VASP code by Martijn Marsman.

KLT RESULTS

We calculated the force constants matrix in KLT40 containing one Li per cell. The reference structure for the force constant calculations was obtained by first placing all ions on ideal perovskite positions and then optimizing lattice parameters and internal coordinates while maintaining full cubic symmetry. The resultant cell had $a = 2 \times 3.956$ Å.

From the force constants, we obtained the dynamical matrix, and the normal mode frequencies and eigenvectors. Symmetry analysis of KLT40 shows 14 Γ_{15} triplets, one which is acoustic and 13 which represent polar transverse optical (TO) modes. In Table 1, we give the TO normal mode frequencies.

TABLE 1. Computed TO normal mode frequencies ν (in cm^{-1}) for cubic $K_7LiTa_8O_{24}$ (KLT). Also shown are relative amplitudes of each mode in the fully relaxed tetragonal KLT structure a_{rel} and relative contributions of each mode to the tetragonal phase polarization P_{rel}

ν	a_{rel}	P_{rel}	ν	a_{rel}	P_{rel}	ν	a_{rel}	P_{rel}
191 *i*	1.0000	0.7225	200	0.0034	0.0023	433	0.0095	0.0005
121	0.1215	0.2330	205	0.0864	0.0384	555	0.0093	0.0129
164	0.0217	0.0014	244	0.0358	0.0080	862	0.0030	0.0003
177	0.0017	-0.0001	337	0.0283	0.0023			
187	0.0806	-0.0212	366	0.0126	-0.0002			

For comparison, we also calculated the force constants of a 40-atom cell of pure KT at the same lattice parameter. The TO normal mode results are shown in Table 2. The force constants in the two cases are nearly identical. The only interatomic force constants which change by more than 0.41 eV/Å^2 are those involving the 12 O ions nearest the Li site, and which favor Li moving against its nearest neighor O sites. In fact, the one lattice instability found in KLT is essentially Li motion (85% of the dynamical matrix eigenvector) opposite its nearest neighbor O (12% of the dynamical matrix eigenvector). Because KLT40 and KT have such similar force constant matrices, it is not surprising that the normal mode spectra are very similar: note that each LO mode in KT has a corresponding KLT40 mode with very similar frequency. Thus, the FP results confirm a picture of KLT in which Li are displaced off-center. We emphasize, however, that a quantitative description of the energetics and dynamics of KLT requires that one also take into account the coordinated motion of the ions surrounding the Li.

TABLE 2. Computed TO normal mode frequencies ν (in cm^{-1}) and dynamical matrix eigenvectors for $KTaO_3$ at $a = 3.956$ Å.

ν	u_K	u_{Ta}	$u_{O\parallel}$	$u_{O\perp}$
115	–0.2989	0.5419	–0.3937	–0.4807
205	0.8745	–0.1737	–0.2401	–0.2715
555	0.0012	0.0341	–0.8531	0.3682

The largest reduction in energy in KLT40 occurs when Li is displaced along a [001] vector. Our results thus support a picture of KLT in which each Li is displaced in one of the 6 [001]-type directions. We performed a full ionic relaxation of KLT, polarized along $\hat{z}$. A breakdown of the displacement pattern into normal mode coordinates is shown in Table 1. Although there is some mixture of higher frequency modes due to anharmonic coupling, the displacement pattern is dominated by the eigenvector of the lattice instability. A more interesting picture emerges when we investigate the contribution of each mode to the polarization of the relaxed structure. Because the 121 cm^{-1} mode corresponding to the soft mode of pure KT has such a large mode effective charge, it contributes 23% of the total polarization of KLT40.

We investigated Li energy as a function of displacement direction and found that the smallest barrier between [001] wells are saddle points in the [110] directions. Fig. 1 shows the energy as a function of Li displacement d in the [001] and [110] directions (see also [7]). Since the barrier energy is comparable with the thermal energy, Li can jump between neighboring [0,0,$\overline{d}$] wells via [110] saddle points.

If all ions except for the Li are fixed, the Li displacements and potential barriers are very small relative those deduced experimentally (by fitting a mean field expansion to experimental data [8]) (upper curves in Fig. 1, see also [7]). However, fully relaxed calculations (lower curves in Fig. 1) yield good agreement: the equilibrium

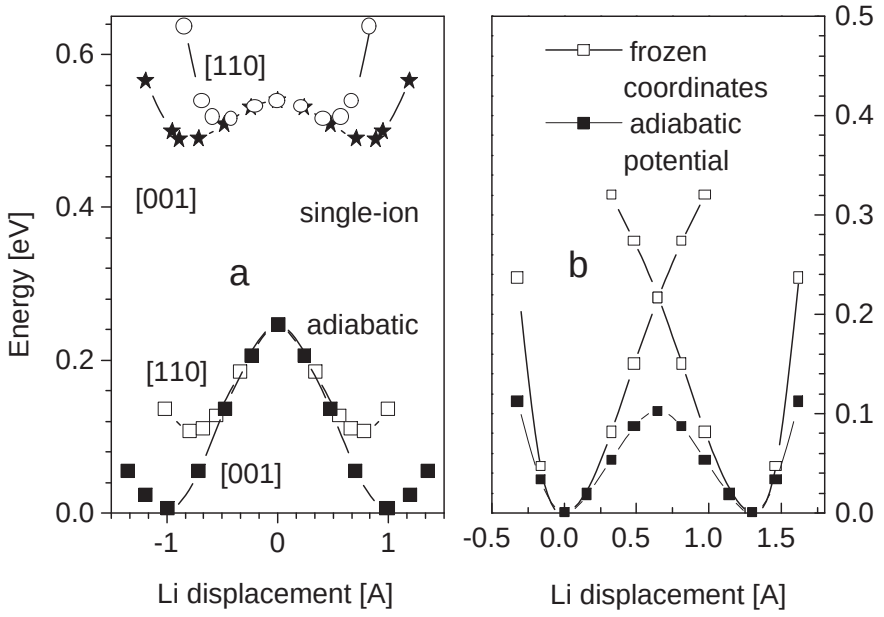


FIGURE 1. Li adiabatic and single-ion potential relief in $KTaO_3$ in [001], [110] directions (a) and in the direction between the Li wells (b)

Li displacement is [0,0,0.99 Å] with $a = 3.96$ Å and [0,0,1.07 Å] with $a = 4.0$ Å; the corresponding adiabatic potential barriers are ∼103 meV (1190 K) and ∼117 meV (1360 K), respectively. The calculated values are somewhat larger than the experimentally estimated barrier of 86 meV (998 K) [8], but they agree rather well with the 1200 K barrier reported by [9]. Computed barrier heights may be systematically larger than fitted values if the latter are reduced by Li-tunneling between neighboring wells over excited states. For the 80 atom supercell we obtained the Li displacement 1.01 Å and the energy barrier U =118 meV (1369 K), which is also somewhat larger than the experimental value of 86 meV (998 K) [8].

Fig. 1(b) represents our computations of Li potential relief along a vector connecting neighboring Li-wells, e.g. [0,0,d] and [0,d,0] via a minimum energy [011] saddle. We computed the "frozen coordinate" (*i.e* all ions frozen except for Li) energies, as well as the adiabatic energies (*i.e* with relaxed coordinates of the non-Li ions). Clearly, ionic relaxation promotes Li-hopping by reducing potential barriers.

In a relaxed supercell, cations displace in the same direction as Li, and anions displace in the opposite direction. This result supports the idea of coupling between Li displacements and ferroelectrically active optical host ion modes [10]. The largest local deformation is exhibited by the four oxygens that are closest to Li. For example, in the 80 atom cell where the Li-displacement is [0,0,1.01 Å], their displacements are [0,-0.074 Å,-0.074 Å]. In the 40 ion supercell these dis-

placements are similar, [0,-0.093 Å,-0.093 Å]. Such distortion was proposed [11] to explain experimental data on the temperature dependence of photocurrent in $[K_{1-x},Li_x]TaO_3$ solid solutions.

These results are in excellent agreement with computations for $LiTaO_3$ and $LiNbO_3$ [12], which also indicated a large oxygen displacements similar to those in our calculations. These oxygen displacments were explained in terms of a reduction in elastic energy that occurs because oxygens prefer to rotate about B site cations rather than directly approaching them [12].

Based on the fact that Li hop over a saddle point, we derived the following expression describing the temperature dependence of the relaxation time:

$$\tau = A \int_{-\infty}^{\infty} e^{\left(U+ay^2\right)/k_BT} dy = A\sqrt{\frac{\pi k_B T}{a}} e^{U(T)/k_BT} = \tau_0\left(T\right) e^{U(T)/k_BT} \tag{1}$$

where: τ is the relaxation time; k_B is the Boltzmann constant; a is a constant. The temperature dependence of the prefactor is a consequence of the existense of different paths when Li overcomes the potential barrier. The temperature dependence of the average barrier, $U(T)$, is governed by the dynamics of the ions surrounding a Li. This dependence can be understood if one introduces spatial and thermal potential barrier fluctuations

$$\begin{aligned} e^{-U(T)/k_BT} &= \frac{\alpha\beta}{\pi k_B T} \int_{-\infty}^{\infty} dx \int_{-\infty}^{\infty} dy\; e^{(U_0+x+y)/k_BT} e^{-\alpha^2x^2-\beta^2(y/k_BT)^2} \\ &= e^{-U_0/k_BT+1/4\beta^2+1/4\alpha^2k_B^2T^2} \end{aligned} \tag{2}$$

From comparison of the left and right sides of this equality one finds $U\left(T\right) = U_0 - k_BT/4\beta^2 - 1/4\alpha^2k_BT$. At high temperature the potential barrier decreases linearly with temperature because of thermal fluctuations (in excellent agreement with experiments performed for $[K_{0.957},Li_{0.043}]TaO_3$ [13]). At low temperatures the barrier height decreases because of spatial fluctuations. Also, critical slowing down of relaxation is common, at low temperature, but in KLT, Li-tunneling is a competitive process [14].

We also performed computations for 80 atom supercells with Li-Li pairs (Fig. 2). A Li-Li pair was introduced into an 80-ion supercell such that nn A-sites (separation vector $a\hat{z}$) were occupied by Li. We considered the following Li-displacement configurations for this pair: (zz), (xx) and $(x\overline{x})$. The energy required to convert a (zz) to $(x\overline{x})$ configuration is 0.27 eV (2990 K) in excellent agreement with the reported barrier height of 2800 K [9,13], attributed to the rearrangement of Li pairs [15]. Significantly, the excitation energy required to move Li pairs into the (xx) configuration, 0.26 eV, is close to the energy required to excite the $(x\overline{x})$ configuration. This occurs because of the indirect dipole-dipole interaction between Li ions in Li-Li pairs over the KT-like soft mode.

The computed dynamical charge of Li in $KTaO_3$:Li is 1.2 e at the equilibrium position but it becomes lower than 1.0 at small Li displacements.

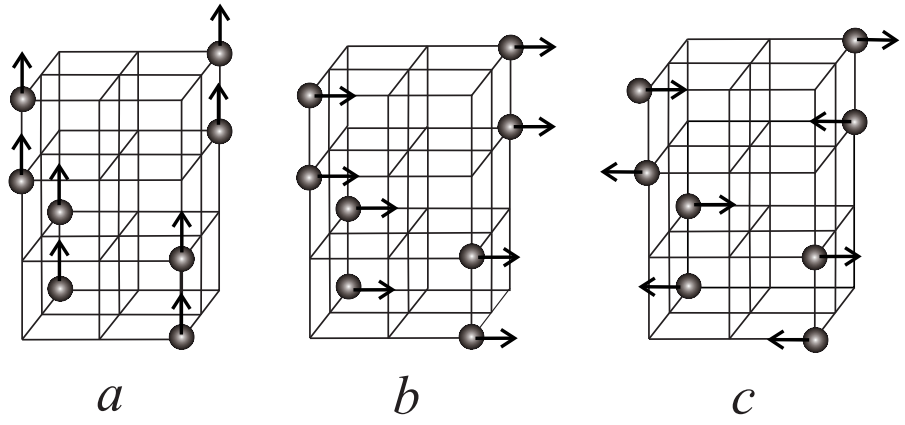


FIGURE 2. A-site configurations in a $[K_{14/16}Li_{2/16}]TaO_3$ supercell (undecorated sites are occupied by K): a) (zz), b) (xx), c) $(x\overline{x})$

KT AND KN RESULTS

The dynamical charges of Ta (Z^*_{Ta}) and Nb (Z^*_{Nb}), in pure KT and KN, respectively, were calculated as functions of [001] displacement in cubic structures with a = 4.015 Å, using a 6x6x6 Monkhorst-Pack k-point grid. The results are shown in Fig. 3.

We also computed electrostatic potentials on the ions and their derivatives. Displacement induced reductions in the second derivative of the potential were consistent with changes in Z^*_{Ta} and Z^*_{Nb}. Indeed one can write a general relation: $E_i(u) = \xi_i(u)Z^*_i u_i$ where $\xi_i(0) \sim 1/\varepsilon_\infty$ and ε_∞ is a high frequency dielectric constant. Hence the reduction in local field (and charge-transfer [1]) that is caused by ionic displacement is responsible for the calculated decrease in dynamical charge. Note that this decrease is rather large: e.g. for Nb in KN Z^*_{Nb} = 9.8 at u=0; 8.5 at u=0.1 Å; and 6.8 at u=0.2 Å.

KTN RESULTS

Results of Z^* computations for KTN supercells are listed in Table 3 and some results for [001] ordered supercells are shown in Fig. 4. Calculations for different [hkl] ordered superstructures, (where [hkl] indicates an ordered sequence of layers perpendicular to the [hkl] vector) were all done with an 8x8x8 Monkhorst-Pack grid. All computations were performed for the *cubic structure* with the fixed lattice parameter a = 3.96 Å. This was done in order to show the pure effect of the neighbors on the dynamical charge. The effect of the ionic displacements were discussed in the previous section.

In the cubic KN, $Z^*_{Nb,zz}$ = 9.9, which is larger than $Z^*_{Ta,zz}$ = 8.8 in KT. Our results are consistent with the studies of Singh [16] which compared covalencies in

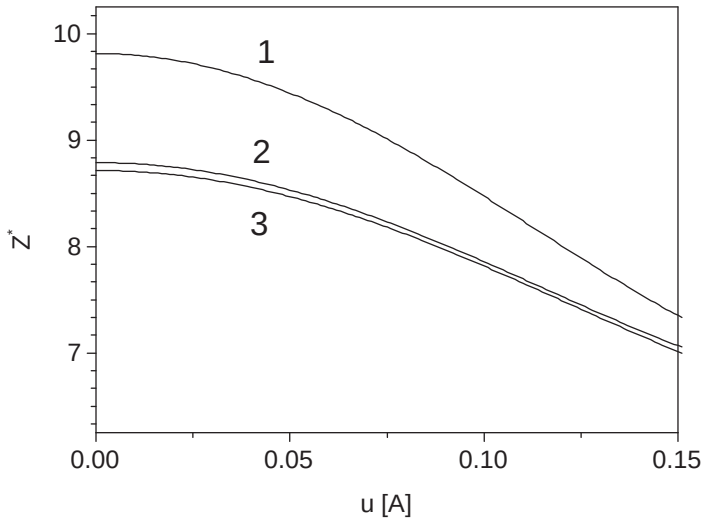


FIGURE 3. Dependence of the dynamical charge on the cation displacement: 1. KN, $a = 4.015$Å. 2. KT $a = 4.015$Å. 3. KT $a = 3.98$Å.

TABLE 3. Dynamical charges in KTN supercells: the first two columns represent the relative numbers of the Nb, x_{Nb}, and Ta, x_{Ta}, planes; the vector [**hkl**] shows the direction perpendicular to the planes.

$\mathbf{x}_{Nb}$	$\mathbf{x}_{Ta}$	[**hkl**]	$Z^*{}_{Nb,zz}$	$Z^*{}_{Nb,xx}$	$Z^*{}_{Ta,zz}$	$Z^*{}_{Ta,xx}$
1	0		9.91	9.91		
0	1				8.79	8.79
1/2	1/2	[001]	9.06	9.88	9.56	8.81
1/3	2/3	[001]	8.78	9.88	9.30	8.80
					9.31	8.81
1/4	3/4	[001]	8.62	9.88	9.18	8.80
					9.23	8.80
					9.16	8.80
2/3	1/3	[001]	9.31	9.89	9.89	8.82
			9.31	9.89		
3/4	1/4	[001]	9.47	9.89	10.06	8.81
			9.41	9.90		
			9.47	9.89		
1/2	1/2	[111]	8.75	8.75	9.22	9.22
1/2	1/2	[110]	9.87	9.23	8.84	9.68

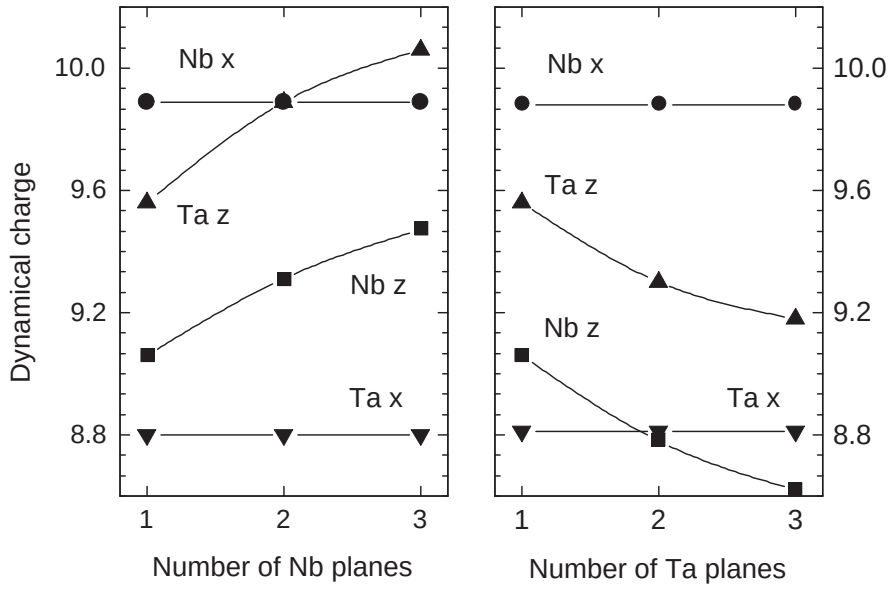


FIGURE 4. Dependence of the dynamical charge on the number of Ta- and Nb- planes in KTN (001) supercells

KT and KN. In layered Nb/Ta superstructures $Z^*_{Nb,zz}$ *decreases* with the number of nn Ta-planes, and $Z^*_{Ta,zz}$ *increases* with the number of nn Nb-planes. Both $Z^*_{B,zz}$'s approach saturation values; $Z^*_{B,xx}$'s, however, exhibit no significant changes. These results are similar to those of previous computations for Nb/Al supercells in $CaTiO_3$-$Ca(Al_{1/2}Nb_{1/2})O_3$ where it was found that the presense of Al decreases the Nb dynamical charge [17].

The effects of cation ordering on Z^* can be well explained via a model in which a layered superstructure is treated as a stacking of slabs with different *local* electronic dielectric permittivities ε_∞. We fit calculated values to the expressions [2]:

$$Z^*_{izz}(N_j) = \frac{\varepsilon_{\infty ij} + 2}{3} g_{ij} \tag{3}$$

where g_{ij} does not depend on the dielectric permittivity. In order to compute the dielectric permittivity in the layered structure considered we used a slightly modified expression for the permittivity of two sequential capacitors

$$\varepsilon_{\infty ij} = \frac{N_{Ta} + N_{Nb}}{N_{Ta}/\varepsilon_{\infty Ta} + \lambda_{ij} N_{Nb}/\varepsilon_{\infty Nb}} \tag{4}$$

Here $\varepsilon_{\infty Nb}$ and $\varepsilon_{\infty Ta}$ are the electronic dielectric permittivities of pure $KNbO_3$ and $KTaO_3$ respectively, N_i $(i = Ta, Nb)$ is the number of Ta- or Nb-planes. This

expression at $\lambda = 1$ is explicit for the simple cubic structure. We fixed $\varepsilon_{\infty Ta}$ at the experimental value 5.15 and, correspondingly, $\lambda_{Ta,Ta} = 1$. Fitting the data in Table 1 yields $\varepsilon_{\infty Nb} = 6.4$, $g_{Ta,Ta} = g_{Ta,Nb} = 3.7$, $g_{Nb,Nb} = g_{Nb,Ta} = 3.5$, $\lambda_{Nb,Nb} = 1$, and $\lambda_{Nb,Ta} = \lambda_{Ta,Nb} = 0.97$. Deviation of the nondiagonal element of λ from 1, and the large values of g, are connected with the difference between the Lorentz field in the simple cubic lattice and that in the perovskite structure. The value of the electronic dielectric permittivity in $KNbO_3$ (6.4) is consistent with that obtained from first principles computation for a cubic structure [18] (6.6).

PMN RESULTS

To further investigate the effects of cation ordering on dynamical charges in complex perovskites, Berry phase analyses were performed for various supercells in the perovskite based system $PbMg_{1/3}Nb_{2/3}O_3$ (PMN); Results are listed in Table 4.

TABLE 4. Dynamical charges Z^*_{ii} in PMN: n.d. are nondiagonal elements where n.d.1 corresponds to nondiagonal elements between [0-11] and [110] while n.d.2 is between [0-11] and [-111].

	PMN [001]		**PMN [110]**			**PMN [111]**			
	[001]	**[100]**	**[001]**	**[-120]**	**n.d.**	**[-111]**	**[0-11]**	**n.d.1**	**n.d.2**
Mg	2.55	1.90	1.90	2.57	–0.06	2.80	2.76	0.00	0.00
Nb	7.63	8.76	8.73	8.23	0.26	6.53	7.13	0.06	0.02
	7.63	8.75	8.69	8.23	0.24	6.50	7.13	0.06	0.00
Pb	3.42	3.80	3.98	4.07	-0.44	4.31	3.76	–0.04	–0.07
	3.32	3.90	3.99	3.60	0.28	3.02	4.31	–0.06	–0.03
	3.38	3.80	3.98	3.53	0.29	4.33	3.78	–0.02	–0.05

As in KTN, the dynamical charges of ions in PMN depend on nn coordination. In particular, Z^*_{Pb} is sensitive to chemical ordering. These results are consistent with Z^*_{Pb}-computations for some other lead relaxors [20]. It is interesting to notice that the largest dynamical charge components for Pb occur in the [111] ordered structure. The nondiagonal elements are generally small compared with the differences between the diagonal elements, which shows that the basis vectors are close to the eigenvectors of the dynamical charge tensor.

CONCLUSIONS

We have computed the minimum energy [110] barrier between adjoining [0,0,d] Li wells in fully relaxed KLT supercells. Our results are in good agreement with values obtained by fitting a mean field expansion to experimental data.

We find that all ions in the supercell are displaced from their ideal positions but among the nn ions, the oxygens closest to Li exhibit the largest sympathetic

displacements; they are displaced in the opposite direction as Li, and move closer to one another. These results support earlier work [11] and computations [12,21].

First-principles computation of Li-Li pair excitations in a $[K_{14/16}Li_{2/16}]TaO_3$ supercell strongly supports a previous assumption [15] about the nature of π-relaxation in KLT. Our low-energy values for excitations of this point defect are in excellent agreement with fits to experimental data.

Computations of the Born charges in KTN and PMN indicate that dynamical charges are sensitive functions of nearest neighbor coordination, which can be explained by heterogeneity in the local electronic dielectric permittivity.

ACKNOWLEDGMENT

We thank G. Kresse for providing an LDA pseudopotential for Ta.

REFERENCES

1. R. Resta, *J.Phys.: Condens. Matter* **12**, R107 (2000).
2. Ph. Ghosez, *Phys. Rev. B* **58**, 6224 (1998).
3. G. Kresse and J. Hafner, *Phys. Rev. B* **47**, 558 (1993).
4. G. Kresse and J. Furthmüller, *Phys. Rev. B* **54**, 11169 (1996).
5. D. J. Singh, *Ferroelectrics* **164**, 143 (1991).
6. G. Shirane, R. Newnham, and R. Pepinsky *Phys. Rev.* **96**, 581 (1954).
7. A. V. Postnikov, T. Neumann and G. Borstel, *Ferroelectrics* **164**, 101 (1995).
8. U. T. Höchli, K. Knorr and A. Loidl, *Adv. Phys.* **39**, 405 (1990).
9. R. K. Pattnaik, J. Toulouse, and B. George *Phys. Rev. B* **62**, 12820 (2000).
10. B. E. Vugmeister and M. D. Glinchuk, *Rev. Mod. Phys.* **62**, 993 (1990).
11. V. V. Laguta, M. D. Glinchuk, I. P. Bykov, J. Rosa, L. Jastrabik, R. S. Klein and G. E. Kugel *Phys. Rev. B* **52**, 7102 (1995).
12. I. Inbar and R. Cohen *Ferroelectrics* **194**, 83 (1997).
13. S. A. Prosandeev, V. A. Trepakov, M. E. Savinov, L. Jastrabik, and S. E. Kapphan *J. Phys.: Condens. Matter* **13**, 9749 (2001).
14. W. Kleemann, V. Shönknecht, D. Sommer, and D. Rytz, *Phys. Rev. Lett.* **66**, 762 (1991).
15. P. Doussineau, Y. Farssi, C. Frenos, A. Levelut, K. McEnaneu, J. Toulouse, S. Ziolkiewicz, *Europhys. Lett.* **24**, 415 (1993).
16. D. J. Singh, Phys. Rev. B **53**, 176 (1996).
17. E. Cockayne, *J. Appl. Phys.* **90**, 1459 (2001).
18. C.-Z. Wang and H. Krakauer, *Ferroelectrics* **194**, 97 (1997).
19. B. P. Burton, *Phys. Rev. B* **59**, 6087 (1999).
20. L. Bellaiche, J. Padilla, and D. Vanderbilt, *Phys. Rev. B* **59**, 1834 (1999).
21. I. I. Tupitsin, A. Deineka, V. A. Trepakov, L. Jastrabik and S. E. Kapphan, *Phys. Rev. B* **64** 195111 (2001).